High-harmonic generation from solids

Shambhu Ghimire* and David A. Reis

High-harmonic generation in atomic gases has been studied for decades, and has formed the basis of attosecond science. Observation of high-order harmonics from bulk crystals was, however, reported much more recently, in 2010. This Review surveys the subsequent efforts aimed at understanding the microscopic mechanism of solid-state harmonics in terms of what it can tell us about the electronic structure of the source materials, how it can be used to probe driven ultrafast dynamics and its prospects for novel, compact short-wavelength light sources. Although most of this work has focused on bulk materials as the source, recent experiments have investigated high-harmonic generation from engineered structures, which could form flexible platforms for attosecond photonics.

Second-harmonic generation is a well-known nonlinear optical phenomenon that can be described by the anharmonic electronic response using perturbation theory. When the strength of the laser field approaches the atomic bonding strength of a material, novel extremely nonlinear optical effects emerge. A canonical example is non-perturbative high-harmonic generation (HHG) in atomic gases, first reported three decades ago[1]. Several aspects of the underlying dynamics of gas-phase HHG can be understood through the three-step recollision model comprising tunnel ionization, free acceleration and recombination[2–4]. The typical spectrum of the emitted radiation consists of odd harmonics with a single plateau stretching out to $I_p + 3.17U_p$, where I_p is the ionization potential of the neutral atom and $U_p = e^2E_0^2\lambda^2/16\pi^2mc^2$ is the ponderomotive energy. Here E_0 and λ are the peak field strength and wavelength of the laser, and e and m are the charge and mass of the electron, respectively. The simplest recollision framework is based on the strong-field approximation[5], which neglects the contribution of the Coulomb potential to the propagation of the tunnel-ionized electrons in the laser field. At high intensity and long wavelength, the approximation works well as the electron trajectories extend far from the parent ion.

Building on this simple picture, gas-phase HHG has formed the basis of attosecond science, which includes probing molecular orbitals[6,7], generation of isolated attosecond pulses[8] and attosecond transient absorption experiments in the gas phase[9] and solid state[10]. While gas-phase HHG has become accessible in research laboratory environments, it still involves expensive complex set-ups including amplified femtosecond lasers, vacuum pumps and means to confine source gas only within the interaction volume, and delicate optics for beam manipulations.

Recently, HHG was also observed in bulk crystals subjected to strong mid-infrared laser fields[11], launching a new field of attosecond and strong-field processes in solids. A schematic of the experimental set-up from ref. [11] is shown in Fig. 1a. High harmonics up to the 25th order were produced in the transmission through a 500-μm-thick ZnO crystal at peak intensity ~5 TW cm^{-2} (field strength ~0.6 V Å^{-1}, pulse energy ~3 μJ), without damage for a repetitive excitation at 1 kHz. The observed spectrum extended beyond the bandgap and comprised a plateau and an abrupt high-energy cutoff, even for the submicrojoule level of laser pulse energy. We note that typical gas-phase HHG sources use millijoule-class pump lasers. More surprisingly, the high-energy cutoff from solids was found to scale linearly with the peak field strength in contrast to the quadratic dependence expected from the three-step recollision model[2–4]. The yield of harmonics deviates strongly from the power law (harmonic order) expected from perturbative nonlinear optics.

Therefore, the ZnO experiment suggested that the solid-state HHG process can be accommodated neither by conventional perturbative nonlinear optics nor by the kinematics of strong-field re-scattering, at least without additional modification from the Coulomb interactions between the densely packed atoms. Subsequent results demonstrated that solid-state HHG can be achieved through a wide variety of interaction media, from wide-bandgap dielectrics[12–16] to novel materials such as graphene[17], with appropriate laser wavelengths from the near-infrared to terahertz range according to the material's bandgap. In addition, several studies pointed out that solid-state HHG could, in principle, probe electronic properties of a wide range of materials, both in and out of equilibrium[18–20]. Therefore, to fully realize the potential of solid-state HHG, it would be desirable to obtain a clear understanding of the underlying microscopic processes, the relationship to the band structure, and macroscopic propagation effects.

Solid-state harmonics are also emerging as a promising route to compact ultrafast and short-wavelength coherent light sources. Stable extreme ultraviolet (XUV) waveforms that are insensitive to the intensity and phase fluctuation of the laser pulse became available[21]. XUV harmonics are observed from the most abundant optical medium, a common glass[22], which means that optical fibres may support generation of attosecond pulses. Below-bandgap harmonics are phase-matched using periodically poled crystals[23]. Recent results indicate that the use of engineered solid structures could manipulate the high-harmonic beam as they are produced[24], suggesting that, finally, the possibility of producing coherent XUV beams directly from the laser oscillator seems within reach.

In this Review, we present a brief overview of the nascent field of solid-state high harmonics. We begin with the recent progress in understanding the underlying physical mechanism, summarize important experimental milestones and conclude with our view on the future of solid-state HHG. For a more detailed update, in particular for the current state-of-the-art of the theory, see the review by Huttner et al.[25].

Strong-field-driven dynamics in solids

It is instructive to consider qualitatively how the microscopic processes involved in solid-state HHG might differ from the standard recollision model. Figure 2 schematically compares the two cases in

Stanford PULSE Institute, SLAC National Accelerator Laboratory, Menlo Park, California, USA. *e-mail: shambhu@slac.stanford.edu

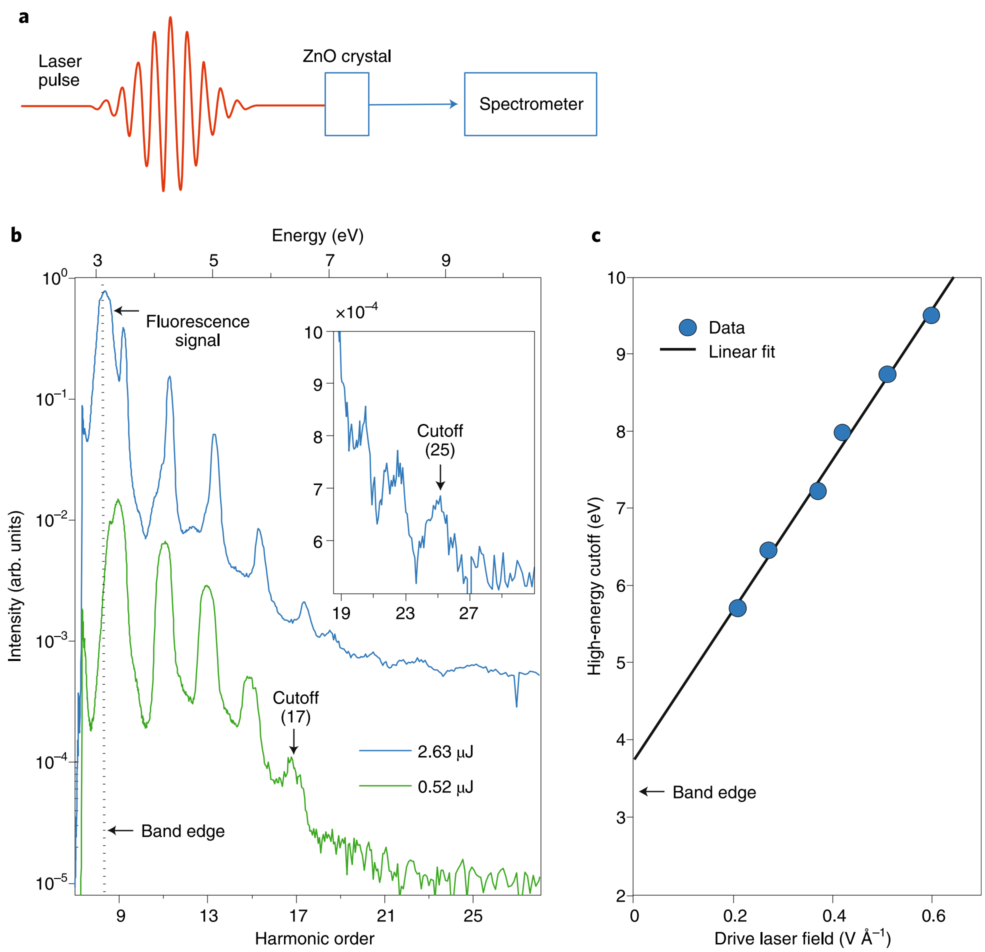

Fig. 1 | High-order harmonic generation in ZnO crystals. a, Schematic diagram of the experimental set-up. A 500-μm-thick sample is pumped by an intense femtosecond mid-infrared laser pulse and high harmonics are collected in transmission using a spectrometer. **b**, Representative measured spectra for two pulse energies. At 0.52 μJ, the spectrum extends to the 17th-order harmonic, which is well beyond the band edge (as shown by the dotted line). At 2.63 μJ, the spectrum extends further to the 25th-order harmonic. The arrows show the locations of abrupt cutoffs. **c**, High-energy cutoff as a function of the peak field, along with a linear fit. The intercept along the energy axis is near the bandgap (3.2 eV). Adapted from ref. [11], Springer Nature Ltd.

both real and momentum (reciprocal) space. The high density of solids means that there is typically significant overlap of neighbouring atomic orbitals, resulting in delocalized valence and conduction band states in crystals. Figure 2a shows how the HHG process in solids might occur in real space. However, it is often convenient to work in reciprocal space using Bloch wavefunctions. In the presence of the laser field, we will make use of the Houston picture[26], where these single-particle states evolve in reciprocal space by replacing the Bloch wavevector $k \rightarrow k(t) = k + e/\hbar \int E(\tau)\,d\tau$. In the absence of scattering, the state moves periodically within a single band, and for strong enough field would diffract from the Brillouin zone boundaries (Bloch oscillations) within a half-cycle at a peak rate given by the Bloch frequency $\omega_B = eE_0/\hbar d$, where d is the lattice constant along the direction of polarization. Also for strong fields, the probability for interband transitions increases and depends exponentially on the instantaneous energy difference between the bands, similarly to Zener tunnelling[27].

Figure 2b schematically shows the electron and hole dynamics in the lowest conduction and highest valance band, respectively. Note that an electron promoted from the valence to the conduction band will never be far from the cores, breaking down the usual strong-field approximation[5]. This is reflected in the non-parabolic shape of the bands, leading to a momentum-dependent group velocity and effective mass (which can take on both positive and negative values). In the Houston picture, both electrons and holes will move together in reciprocal space following the vector potential of the light. Therefore, in solids there are two major possibilities: radiation from nonlinearities in the intraband current including through Bloch oscillations[13,28,29], and emission from interband polarization[30–32]. A mixed-basis approach was taken by Osika et al.[33], using Wannier (real-space) wavefunctions for the valence-band holes and Bloch wavefunctions for the conduction-band electrons.

For comparison, it is useful to convert the nominal real-space picture of atomic HHG (see Fig. 2c) into the momentum space (see Fig. 2d). First, the electron tunnels to the continuum, with zero momentum. Then, the electron moves within the continuum following a parabolic dispersion as it acquires kinetic energy from the laser field. Finally, the electron returns to the parent ion, typically with high momentum (and thus kinetic energy), whose exact value depends on both the ionization and recombination time. Note that, compared to the electron, the ionic dispersion is flat. During the recombination process, high-energy photons are released in the form of high-order harmonics as this process repeats over many laser cycles. It is important to note that there is no analogue to the nonlinear intraband current in the three-step recollision model of atomic HHG, although in both cases the stepwise population increase in the multicycle pulse could also give rise to relatively low-order harmonic radiation[34].

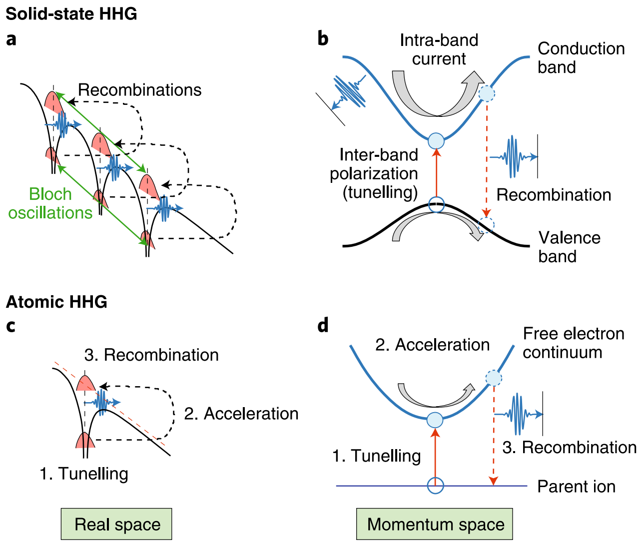

Fig. 2 | Microscopic mechanisms for atomic and solid-state HHG. **a**, The real-space picture with several possibilities; the driven electron could scatter from the periodic Coulomb potential termed as Bloch oscillations, recombine with the associated hole (ion) and recollide with the first- and second-nearest holes (ions) because of closely packed atoms. Periodic arrays of atoms in a crystal exhibit a collective response. **b**, The momentum-space version of **a** using simple cosine bands, showing intraband Bloch oscillations in the conduction band and interband coupling between the valance band and the conduction band, both emitting high-frequency radiation in the forward direction. **c**, Schematic diagram of the three-step recollision model comprising tunnel ionization, free-acceleration and recombination. **d**, The momentum-space version of **c**, where the electron tunnels from the bound state to the continuum state, accelerates in the parabolic continuum band and then recombines to the bound state (parent ion) emitting high-frequency radiation.

The original ZnO results were interpreted as being consistent with the radiation from the nonlinear intraband current arising from (a.c.) Bloch oscillations of the tunnel-ionized electrons repeating on each half laser cycle[11]. In this picture, one would predict non-perturbative harmonics with a high-energy cutoff that is proportional to the peak Bloch frequency and thus linear in the electric field. Multiple cutoffs given by the various Fourier coefficients of the band would also be predicted. In subsequent work by Luu et al., this dependence was used to extract the conduction-band structure for SiO_2 from the harmonic spectra[13]. In addition, calculations showed that the time-frequency profiles of high harmonics are markedly different depending on whether they arise from the nonlinear interband polarization or the nonlinear intraband currents[35].

While the interband and intraband dynamics are intimately coupled, particularly at high fields, the identification of their relative roles is relevant to many applications such as probing electronic structures and attosecond pulse generation. One important difference is that the microscopic intraband emission is expected to be effectively chirp-free compared to interband emission that involves a chirp that depends on both laser parameters and band structure. Propagation effects could also add an additional chirp through dispersion[36] and self-phase modulation of the laser pulse. In ZnO films, atto-chirp was measured through high-harmonic spectroscopy, where a significantly weak second-harmonic field gently perturbs the generation process[37]. As the second-harmonic field breaks the symmetry, even-order harmonics are produced with an intensity that depends on the two-colour phase delay. Their modulation was found to depend on the harmonic order, revealing existence of atto-chirp. In contrast, high harmonics from crystalline SiO_2 are found to be not-recollision-like and are best described using the nonlinear (a.c.) Bloch oscillations as the dominating mechanism[21,38]. In the interband model, the two-colour techniques can recover the momentum-dependent bandgap[18]. The detail of the solid-state HHG mechanism remains a highly debated topic[13,15,28,32,33,36,37,39,40].

Progress towards shorter wavelengths

In HHG from gases, it is well established that the high-energy cutoff scales quadratically with the wavelength and peak field strength of the laser pulse, and depends only weakly on the target atom through the ionization potential, as expected from the single-atom recollision picture[2–4]. Therefore, much of the efforts towards cutoff extension are focused on using a longer-wavelength pump, and gas-phase HHG has reached the soft-X-ray wavelength range. In solid-state HHG, the cutoff scales linearly to the peak field[11] and it also depends strongly on the electronic band structure[13,30]. According to the interband model, the cutoff should be limited to the maximum bandgap at the Brillouin zone edge[18,31]. In this picture, a new plateau and associated cutoff is expected for higher fields as the driven electron acquires enough energy to climb up into higher conduction bands[39]. In the intraband model, the bandgap limit does not exist[11,13,28]; however, for high enough peak fields, the electrons may still tunnel to high-lying conduction bands[27]. Therefore, for both contributions, multiple plateaus are possible either through the shape of the lowest conduction band (intraband)[11,13] or through the number of involved bands including high-lying conduction bands (interband)[14,41].

Figure 3 shows the wide range of source materials, pump laser wavelengths and reported approximate high-harmonic cutoff energies. It can be seen that narrow-bandgap materials are suitable for terahertz and mid-infrared pumps, while wide-bandgap dielectrics can be pumped by strong near-infrared lasers without sample damage. As discussed above, Zener tunnelling depends exponentially on the bandgap, so higher-bandgap materials have a higher breakdown threshold. Luu et al.[13] reported XUV harmonics from crystalline SiO_2 pumped by 1.5 cycle ~800 nm laser pulses of intensity ~16 TW cm^{-2}. A subsequent study showed that that XUV harmonics from quartz crystals are chirp-free, consistent with the generation from intraband nonlinear current[38]. Ndabashimiye et al.[14] produced high harmonics in the XUV photon energy range from frozen Ar and Kr, including direct comparisons to their gas phase counterparts. In those experiments, polycrystalline Ar films are pumped by ~50 fs, ~1,300 nm pulses of peak intensities ~26 TW cm^{-2} without damage. Multiple plateaus are observed in high-harmonic spectra from both solid Ar (bandgap 14.3 eV) and Kr (bandgap 11.6 eV) extending to ~40 eV, which is beyond the gas-phase cutoff measured under similar conditions. Multiple plateaus are shown to be a general feature of solid-state HHG that could yield important information about the electronic structure of materials. For example, in a subsequent work, You et al. also observed a secondary plateau on high-harmonic spectra from crystalline MgO (ref. [41]) and crystalline SiO_2 (ref. [22]). Moreover, the high-energy cutoff of the primary plateau in MgO was found to be equal to the bandgap at the Brillouin zone edge, consistent with the prediction from the interband model.

Generation of XUV harmonics from amorphous common glass[22] indicates the possibility of using a wide range of readily available optical media. Normally, the high-energy cutoff is limited by materials damage at high intensities. Using ultrashort laser pulses could thus increase the damage threshold. Moreover, there is strong self-absorption of the XUV photons by the source material. Typically, attenuation lengths in the XUV wavelength range are just tens of nanometres; however, it might be possible to mitigate the absorption by working just below the absorption edge of materials. For example, for Si the attenuation length at around 98 eV (just below the L_3 edge) is ~500 nm. It was also recently shown that bulk HHG could take advantage of reflection geometry[42].

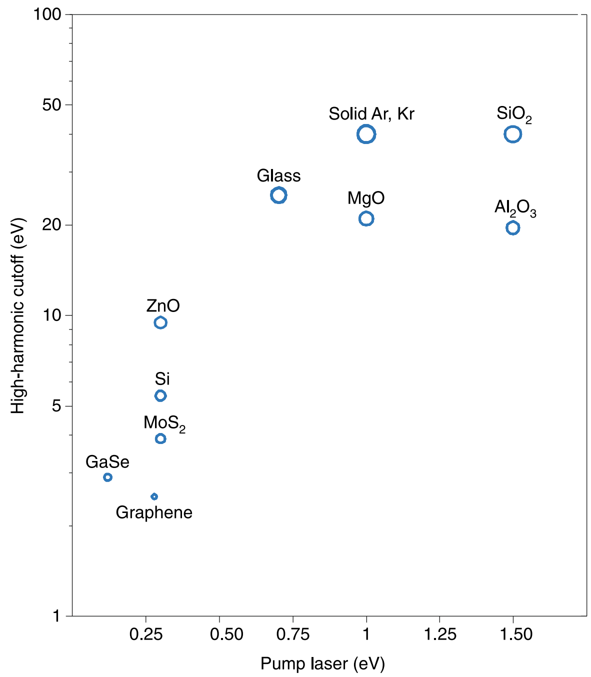

Fig. 3 | Recent progress in high harmonics from solids. The photon energy of the highest-order harmonic observed from a wide range of materials. Metals and semiconductors need terahertz or mid-infrared fields because of the smaller bandgap. Generation from wide-bandgap dielectrics reaches XUV photon energy, as they can be pumped by near-infrared laser fields and with higher peak fields because of the higher damage threshold. The size and location of the circle approximately respectively represent the bandgap and high-energy cutoff. The materials are, in ascending order: graphene[17], GaSe (ref. [12]), MoS_2 (ref. [49]), Si (ref. [54]), ZnO (ref. [11]), MgO (ref. [41]), glass[22], Al_2O_3 (ref. [16]), SiO_2 (ref. [13]), solid Kr and solid Ar (ref. [14]).

Carrier-envelope phase control

The role of carrier-envelope phase (CEP) could be important when the driving laser pulse is short and has only a few cycles. Schubert et al.[12] observed CEP dependence on high harmonics from bulk GaSe crystals pumped by strong few-cycle terahertz pulses. A representative spectrum is shown in Fig. 4a. The analysis of the dependence of the high-harmonic spectrum on CEP could reveal important information about the underlying microscopic mechanism. In a two-band model, interband harmonics are emitted when the harmonic photon energy matches the instantaneous field-dressed bandgap[39,41], $\varepsilon(t) = 2\hbar\sqrt{(\mu E(t))^2 + (\omega_o/2)^2}$, where μ is the transition dipole matrix element, $E(t)$ is the time-dependent field and ω_o is the bandgap. In the few-cycle limit, there would be a large variation in the amplitude of the laser field in consecutive half-cycles. Therefore, if a value of $\varepsilon(t)$ is reached at a particular time t in a half-cycle, in the subsequent half-cycle the same value can be reached earlier (or later) than $t + T/2$, where T is the laser period. This causes a phase delay between the photons of the same energy originating from different half-cycles. You et al.[41] showed that this subcycle delay gets manifested in the form of a significant shift in the photon energy of high harmonics (CEP shift, from here on). A strong CEP shift in the photon energy was observed in XUV harmonics from MgO crystals: a portion of the results is shown in Fig. 4b, where the CEP shift is marked by a dotted line near the end of the primary plateau at around 18 eV. It is remarkable that the secondary plateau also shows a strong CEP shift, indicating that the higher-lying conduction bands also get populated in the subcycle timescale.

In contrast, the pure intraband model does not predict a CEP shift. This is because in the time domain all harmonics are in phase, essentially with no atto-chirp[31,36]. In fact, very recently You et al.[41] and Garg et al.[21] observed that the photon energy of high harmonics from crystalline SiO_2 does not change with CEP in two independent experiments, at ~1,600 nm and ~800 nm pump laser wavelengths, respectively. A portion of results from SiO_2 is shown in Fig. 4c. We note that in the gas phase, the CEP dependence is also strong, but it is largely independent of the target atom. The material-dependent response in solids is thus striking and should be investigated in detail. In crystal quartz, the observation of the relative insensitivity of high harmonics and thus of the XUV pulse waveform to the intensity and phase noise of the pump laser could be attractive for metrology applications[21]. Similarly, a strong CEP dependence, as observed in MgO crystal in the interband model, could be useful to control and probe multiband-driven electron dynamics in solids[43].

Atomic-scale structural sensitivity

Understanding the mechanism for solid-state HHG from a real-space perspective could lead to novel approaches for studying materials at the atomic level with light. For example, in analogy with molecular orbital tomography experiments in the gas phase[6], solid-state HHG could be utilized to probe valance charge density and even the wavefunctions in the condensed phase. Strong-field-driven electrons could scatter coherently off the periodic potential on subcycle timescales, such that HHG is completed nominally well before the lattice motion becomes appreciable. As for HHG in aligned diatomic molecules[44], You et al.[15] found that high harmonics from MgO depend strongly on the orientation of the crystal with respect to the laser field. The efficiency is enhanced when the field is along the interatomic bonding directions. They also observed a rich ellipticity dependence, which includes generation with strong elliptically polarized fields. Analysing the semiclassical electron trajectories in real space may elucidate the microscopic origin of this anisotropy. In this case, You et al.[15] found that the efficiency of high harmonics is enhanced (diminished) when the trajectories connect (miss) the first- and second-nearest-neighbour atomic cores. Subsequently, the real-space picture of solid-state HHG has been applied to probe the periodic potential of the crystal in three dimensions[45]. It might be possible to implement wavefunction reconstruction procedures similar to molecular HHG[46]. In the gas phase, HHG efficiency drops abruptly when ellipticity is introduced as the returning electron is deflected away from the associated parent ion. Apparently, this is also true in rare gas solids[14], probably because the atoms are held together by weak van der Waals forces and thus the valence charge distribution is fairly concentrated around the atomic cores. Therefore, we suggest that the real-space picture could be highly useful in investigating the possibility of imaging single atomic sites in solids. An implication for the study of materials could be, for example, the optical inspection of impurities and vacancies in semiconductors and dielectrics.

Harmonics from nanoscale structure

Another exciting aspect of high harmonics from solids is the possibility of designing engineered structures and using two-dimensional materials to control properties of high harmonics. Structures could be designed with appropriate chemical composition and morphology to control the local field and consequently the generation process. Han et al.[47] showed that the surface-plasmon-enhanced local fields in a gold–sapphire nanostructure enhance the incident laser field and produce non-perturbative high harmonics. As a result of the local enhancement, harmonics up to the 13th order are produced directly from the laser oscillator at 75 MHz repetition rates. The design of the metal–sapphire tip and the measured spectrum are shown in Fig. 5a,b. In a subsequent work, Vampa et al.[48] demonstrated the use of an array of gold monopole nano-antennas to enhance the generation efficiency in silicon by about 5 to 10 times. These remarkable experimental results demonstrate clearly that the

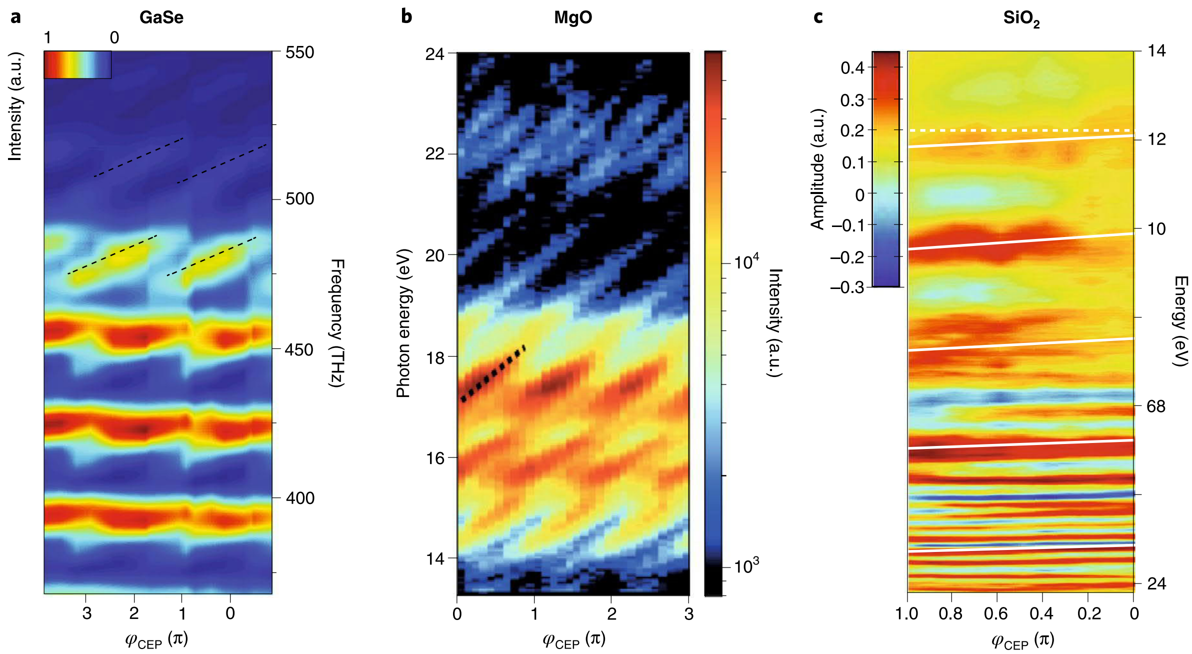

Fig. 4 | CEP dependence of high-order harmonics from various solid materials. a, A GaSe crystal pumped by a terahertz pulse. The photon energy shift is represented by a dotted line. **b**, A MgO crystal pumped by an optical parametric chirped-pulse amplification laser at ~1,600 nm. The photon energy shift is represented by a black dotted line. A strong shift can be seen in both the primary and secondary plateaus. **c**, A SiO_2 crystal pumped by a Ti:sapphire laser at ~800 nm, where the harmonic photon energy does not change as a function of CEP setting. Adapted from ref. [12], Springer Nature Ltd (**a**); ref. [41], OSA (**b**); and ref. [21], Springer Nature Ltd (**c**).

nanoscale engineering of solid materials could be a powerful way to control the generation processes and maybe even optimize the properties of high harmonics such as their polarization and temporal structure. Sivis et al.[24] produced and focused high harmonics from an integrated Fresnel zone plate. The zone plate consists of ten implanted zones, which show enhanced generation as compared to the unmodified zones. Figure 5c shows a picture of the zone plate along with its scanning electron microscopy image in the inset, and Fig. 5d shows the micrometre-sized focus spots of the individual harmonics. Many applications require focusing high harmonics to a small spot, and that is a challenging task particularly in the XUV wavelength range. The use of large-bandgap dielectrics such as MgO on these devices could extend this approach to the XUV wavelength range. The use of metamaterials could also be exploited to phase-match XUV harmonics.

The use of two-dimensional materials such as graphene and transition-metal dichalcogenides could confine the underlying dynamics to a reduced dimension. In these materials, the generation can be influenced by linear dispersion, tunable bandgap including zero bandgap at the zone centre, different symmetries and enhanced many-body interactions due to lack of screening. Liu et al.[49] observed high harmonics from isolated single-layer MoS_2 subject to mid-infrared laser pulses of peak intensity 2.2 TW cm^{-2} without damage. The spectrum from the single layer consists of both odd- and even-order harmonics, while bulk MoS_2 produces only odd-order harmonics. The polarization of the even orders is orthogonal to the polarization of the laser field, indicating a novel mechanism. This could be explained in part due to the contribution from the anomalous nonlinear current driven by the material's Berry curvature. Moreover, the per-layer efficiency of the emission from an isolated layer is much higher than that from the bulk, indicating the importance of strong Coulomb interactions in the reduced dimension. In a subsequent work, Yoshikawa et al.[17] observed HHG from single-layer graphene pumped by mid-infrared laser pulses at peak intensity 1.7 TW cm^{-2} without damage. These experimental results point to the possibility of strong-field and attosecond physics in reduced-dimension and engineered materials.

Future prospective and challenges

In less than a decade, high harmonics from solids has emerged as a frontier of strong-field and attosecond science. The availability of few-cycle, high-intensity pulses in the long-wavelength range allows for the application of large fields, comparable to the bandgap per lattice constant, while avoiding sample damage. With the use of long-wavelength lasers, multiphoton ionization can be suppressed in a wide range of materials. Rapid progress in near- and mid-infrared laser systems including those based on optical parametric chirped-pulse amplification techniques will allow for more controlled experiments, including reaching higher repetition rates and using nanoscale materials. These experiments will have tremendous impact for all solid-state compact short-wavelength sources, as well as for all-optical strong-field and subcycle probes of electronic structures and dynamics in complex materials.

For example, the potential for subfemtosecond pulses in the vacuum ultraviolet wavelength range could allow table-top photoemission and ultrafast molecular dynamics, especially when combined with repetition-rate pump lasers. These novel ultrafast tools could be useful to generate and probe light-induced electronic states such as Floquet states in topologically relevant materials[50]. Robust, all-optical, table-top methods to image valance charge density in bulk materials could also emerge. We note that several attosecond optics methods previously implemented in the gas-phase HHG[51], such as polarization gating, amplitude gating and the attosecond lighthouse, could also be extended to solid-state HHG. The advantage of the solid state is the possibility of polarization control in high harmonics[52], including orthogonal pulse trains[53].

In the future, we expect to see more time-domain measurements, where the HHG process can be controlled. High-harmonic

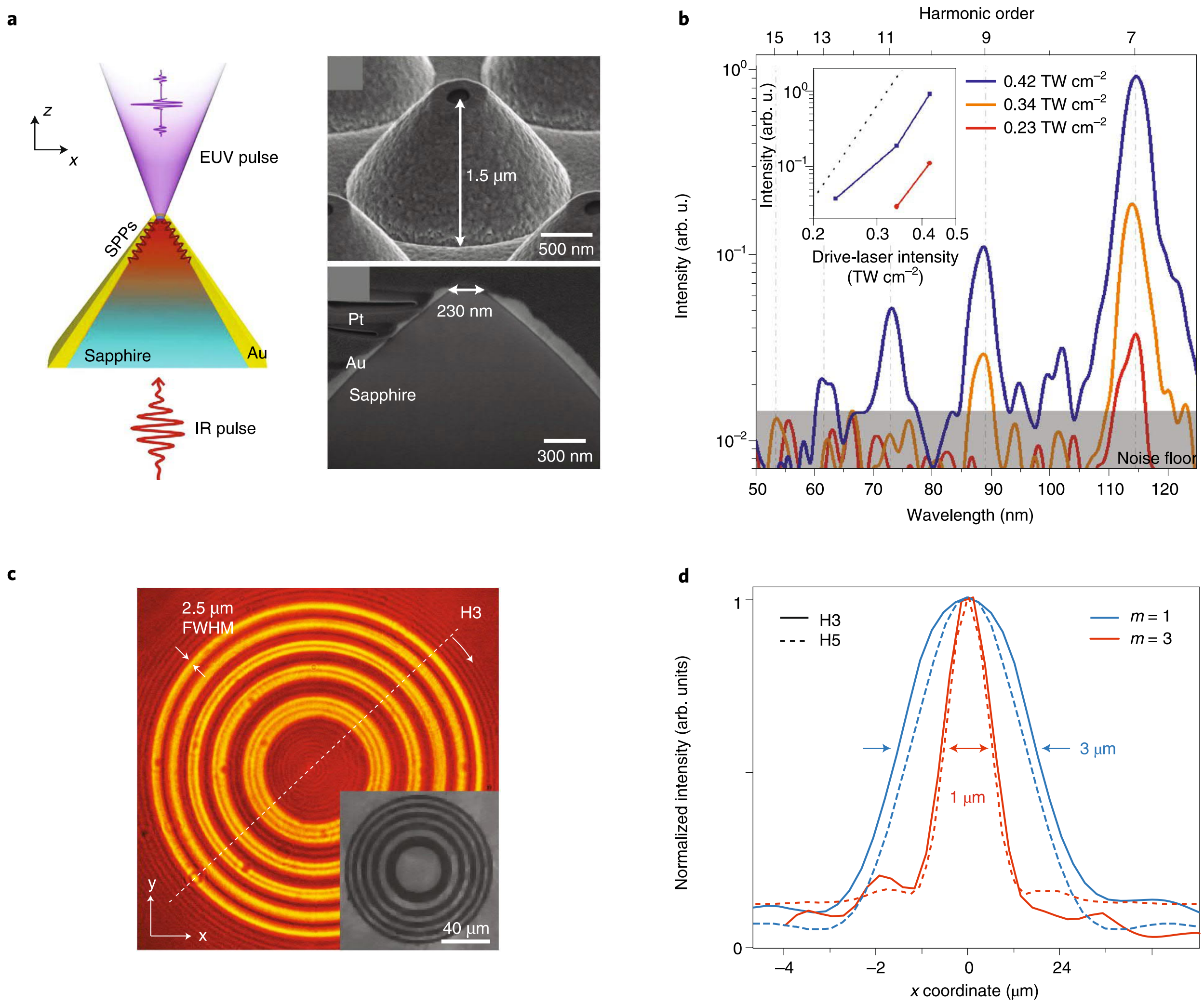

Fig. 5 | The use of engineered solid materials to generate and manipulate high harmonics. **a**, A conceptual schematic diagram of the field enhancement by surface plasmon polaritons (SPPs) on a metal–sapphire nanotip (left) and a scanning electron microscopy image of the structure (right). **b**, Measured high-harmonic spectra at different peak intensities. The inset shows the intensity scaling of 7th-order (blue) and 9th-order (red) harmonics along with 7th-order power law (dotted line). **c**, A gallium-implanted zone plate pattern on silicon along with its scanning electron microscopy image in the inset. FWHM, full-width at half-maximum. **d**, Intensity line-outs at the focus spot of the third- and fifth-order harmonics, showing the focusing ability. Adapted from ref. [47], Springer Nature Ltd (**a**,**b**); and ref. [24], AAAS (**c**,**d**).

spectroscopy could include surfaces, nanoscale materials and metamaterials. It has been shown that HHG can be modified by small external electric fields[54], which are available within operating electrical devices and electronics. Therefore, this feature of solid-state HHG could be implemented towards high-resolution imaging of flowing charge in electrical circuits.

It is well known that ultrafast processes in condensed matter require consideration of electron–electron scattering and in many cases other correlations. While results from MoS_2 and the rare gas solids have hinted at correlation effects, and electron-hole dephasing has been included phenomenologically in various models, so far solid-state HHG has been understood largely using single-active-electron approximation. Thus, there is a need for predictive theories that include electron correlations[19].

Finally, a unique challenge of the solid state is an appropriate understanding of propagation effects such as self-phase modulation of the laser pulse in terms of consequent modifications to spatiotemporal characteristics of high harmonics. By choosing appropriate thicknesses, the nonlinear phase shift acquired from self-phase modulation could be employed to manipulate the relative emission phase of high harmonics and temporally shape the emitted radiation.

Received: 7 February 2018; Accepted: 13 September 2018;
Published online: 19 November 2018

References

1. Ferray, M. et al. Multiple-harmonic conversion of 1064 nm radiation in rare gases. *J. Phys. B* **21**, L31 (1988).
2. Krause, J. L., Schafer, K. J. & Kulander, K. C. High-order harmonic generation from atoms and ions in the high intensity regime. *Phys. Rev. Lett.* **68**, 3535–3538 (1992).
3. Schafer, K. J., Yang, B., DiMauro, L. F. & Kulander, K. C. Above threshold ionization beyond the high harmonic cutoff. *Phys. Rev. Lett.* **70**, 1599–1602 (1993).
4. Corkum, P. B. Plasma perspective on strong field multiphoton ionization. *Phys. Rev. Lett.* **71**, 1994–1997 (1993).
5. Reiss, H. R. Complete Keldysh theory and its limiting cases. *Phys. Rev. A* **42**, 1476–1486 (1990).
6. Itatani, J. et al. Tomographic imaging of molecular orbitals. *Nature* **432**, 867–871 (2004).
7. McFarland, B. K., Farrell, J. P., Bucksbaum, P. H. & Guhr, M. High harmonic generation from multiple orbitals in N_2. *Science* **322**, 1232–1235 (2008).

8. Baltuška, A. et al. Attosecond control of electronic. *Nature* **421**, 611–615 (2003).
9. Goulielmakis, E. et al. Real-time observation of valence electron motion. *Nature* **466**, 739–743 (2010).
10. Schultze, M. Attosecond band-gap dynamics in silicon. *Science* **346**, 1348–1352 (2014).
11. Ghimire, S. et al. Observation of high-order harmonic generation in a bulk crystal. *Nat. Phys.* **7**, 138–141 (2011).
12. Schubert, O. et al. Sub-cycle control of terahertz high-harmonic generation by dynamical Bloch oscillations. *Nat. Photon.* **8**, 119–123 (2014).
13. Luu, T. T. et al. Extreme ultraviolet high-harmonic spectroscopy of solids. *Nature* **521**, 498–502 (2015).
14. Ndabashimiye, G. Solid-state harmonics beyond the atomic limit. *Nature* **534**, 520–523 (2016).
15. You, Y. S., Reis, D. A. & Ghimire, S. Anisotropic high-harmonic generation in bulk crystals. *Nat. Phys.* **13**, 345–349 (2017).
16. Kim, H., Han, S., Kim, Y. W., Kim, S. & Kim, S.-W. Generation of coherent extreme-ultraviolet radiation from bulk sapphire crystal. *ACS Photon.* **4**, 1627–1632 (2017).
17. Yoshikawa, N., Tamaya, T. & Tanaka, K. High-harmonic generation in graphene enhanced by elliptically polarized light excitation. *Science* **356**, 736–738 (2017).
18. Vampa, G. et al. All-optical reconstruction of crystal band structure. *Phys. Rev. Lett.* **115**, 193603 (2015).
19. Silva, R. E. F., Blinov, I. V., Rubtsov, A. N., Smirnova, O. & Ivanov, M. High-harmonic spectroscopy of ultrafast many-body dynamics in strongly correlated systems. *Nat. Photon.* **12**, 266–270 (2018).
20. Wu, M., Ghimire, S., Reis, D. A., Schafer, K. J. & Gaarde, M. B. High-harmonic generation from Bloch electrons in solids. *Phys. Rev. A* **91**, 043839 (2015).
21. Garg, M., Kim, H. Y. & Goulielmakis, E. Ultimate waveform reproducibility of extreme ultraviolet pulses by high harmonic generation in bulk dielectrics. *Nat. Photon.* **12**, 291–296 (2018).
22. You, Y. S. et al. High-harmonic generation in amorphous solids. *Nat. Commun.* **8**, 724 (2017).
23. Park, H. et al. High-order harmonic generations in intense mid IR fields by cascade 3-wave mixing in a fractal-poled $LiNbO_3$ photonic crystal. *Opt. Lett.* **42**, 4020–4023 (2017).
24. Sivis, M. et al. Tailored semiconductors for high-harmonic optoelectronics. *Science* **357**, 303–306 (2017).
25. Huttner, U., Kira, M. & Koch, S. W. Ultrahigh off-resonant field effects in semiconductors. *Laser Photon. Rev.* **11**, 1700049 (2017).
26. Houston, W. V. Acceleration of electrons in a crystal lattice. *Phys. Rev.* **57**, 184–186 (1940).
27. Zener, C. A theory of the electrical breakdown of solid dielectrics. *Proc. R. Soc. Lond. A* **145**, 523–529 (1934).
28. Golde, D., Meier, T. & Koch, S. W. High harmonics generated in semiconductor nanostructures by the coupled dynamics of optical inter- and intraband excitations. *Phys. Rev. B* **77**, 75330 (2008).
29. Ghimire, S. et al. Redshift in the optical absorption of ZnO single crystals in the presence of an intense midinfrared laser field. *Phys. Rev. Lett.* **107**, 167407 (2011).
30. Vampa, G. Theoretical analysis of high-harmonic generation in solids. *Phys. Rev. Lett.* **113**, 73901 (2014).
31. Wu, M., Ghimire, S., Reis, D. A., Schafer, K. J. & Gaarde, M. B. High-harmonic generation from Bloch electrons in solids. *Phys. Rev. A* **91**, 043839 (2015).
32. Hawkins, P. G., Ivanov, M. Y. & Yakovlev, V. S. Effect of multiple conduction bands on high-harmonic emission from dielectrics. *Phys. Rev. A* **91**, 013405 (2015).
33. Osika, E. N. et al. Wannier-Bloch approach to localization in high-harmonics generation in solids. *Phys. Rev. X* **7**, 021017 (2017).
34. Brunel, F. Harmonic generation due to plasma effects in a gas undergoing multiphoton ionization in the high-intensity limit. *J. Opt. Soc. Am. B* **7**, 521–526 (1990).
35. Wu, M., Ghimire, S., Reis, D. A., Schafer, K. J. & Gaarde, M. B. High-harmonic generation from Bloch electrons in solids. *Phys. Rev. A* **91**, 43839 (2015).
36. Ghimire, S. Generation and propagation of high-order harmonics in crystals. *Phys. Rev. A* **85**, 43836 (2012).
37. Vampa, G. et al. Linking high harmonics from gases and solids. *Nature* **522**, 462–464 (2015).
38. Garg, M. et al. Multi-petahertz electronic metrology. *Nature* **538**, 359–363 (2016).
39. Wu, M., Browne, D. A., Schafer, K. J. & Gaarde, M. B. Multi-level perspective on high-order harmonic generation in solids. *Phys. Rev. A* **94**, 063403 (2016).
40. Higuchi, T., Stockman, M. I. & Hommelhoff, P. Strong-field perspective on high-harmonic radiation from bulk solids. *Phys. Rev. Lett.* **113**, 213901 (2014).
41. You, Y. S. et al. Laser waveform control of extreme ultraviolet high harmonic generation in solids. *Opt. Lett.* **42**, 1816–1819 (2017).
42. Vampa, G., Ou, Y. S. Y., Iu, H. L., Ghimire, S. & Reis, D. A. Observation of backward high-harmonic emission from solids. *Opt. Express* **26**, 12210–12218 (2018).
43. You, Y. et al. Laser waveform control of extreme ultraviolet high harmonics from solids. *Opt. Lett.* **42**, 1816–1819 (2017).
44. Velotta, R., Hay, N., Mason, M. B., Castillejo, M. & Marangos, J. P. High-order harmonic generation in aligned molecules. *Phys. Rev. Lett.* **87**, 183901 (2001).
45. You, Y. S., Cunningham, E., Reis, D. A. & Ghimire, S. Probing periodic potential of the crystal via strong-field re-scattering. *J. Phys. B* **51**, 114002 (2018).
46. Itatani, J. et al. Tomographic imaging of molecular orbitals. *Nature* **432**, 867–871 (2004).
47. Han, S. et al. High-harmonic generation by field enhanced femtosecond pulses in metal-sapphire nanostructure. *Nat. Commun.* **7**, 13105 (2016).
48. Vampa, G. et al. Plasmon-enhanced high-harmonic generation from silicon. *Nat. Phys.* **13**, 659–662 (2017).
49. Liu, H. et al. High-harmonic generation from an atomically thin semiconductor. *Nat. Phys.* **13**, 262–265 (2016).
50. Wang, Y. H., Steinberg, H., Jarillo-Herrero, P. & Gedik, N. Observation of Floquet-Bloch states on the surface of a topological insulator. *Science* **342**, 453–457 (2013).
51. Chang, Z., Corkum, P. B. & Leone, S. R. Attosecond optics and technology: progress to date and future prospects [Invited]. *J. Opt. Soc. Am. B* **33**, 1081–1097 (2016).
52. Saito, N. et al. Observation of selection rules for circularly polarized fields in high-harmonic generation from a crystalline solid. *Optica* **4**, 1333–1336 (2017).
53. Langer, F. et al. Symmetry-controlled temporal structure of high-harmonic carrier fields from a bulk crystal. *Nat. Photon.* **11**, 227–231 (2017).
54. Vampa, G. et al. Strong-field optoelectronics in solids. *Nat. Photon.* **12**, 465–468 (2018).

Acknowledgements

This work is supported by the US Department of Energy, Office of Science, Basic Energy Sciences, Chemical Sciences, Geosciences, and Biosciences Division, primarily through the Early Career Research Program (S.G.). D.A.R. was supported through AMOS programme.

Competing interests

The authors declare no competing interests.